JACS
JOURNAL OF THE AMERICAN CHEMICAL SOCIETY

Communication

pubs.acs.org/JACS

Synthesis of Two-Dimensional $CoS_{1.097}$/Nitrogen-Doped Carbon Nanocomposites Using Metal–Organic Framework Nanosheets as Precursors for Supercapacitor Application

Feifei Cao,[†,‡,∥] Meiting Zhao,[‡,∥] Yifu Yu,[‡] Bo Chen,[‡] Ying Huang,[‡] Jian Yang,[‡] Xiehong Cao,[‡,§] Qipeng Lu,[‡] Xiao Zhang,[‡] Zhicheng Zhang,[‡] Chaoliang Tan,[‡] and Hua Zhang*[,‡]

[†]College of Science, Huazhong Agricultural University, No. 1 Shi-zi shan Street, Wuhan, 430070, China

[‡]Center for Programmable Materials, School of Materials Science and Engineering, Nanyang Technological University, 50 Nanyang Avenue, Singapore 639798, Singapore

[§]College of Materials Science and Engineering, Zhejiang University of Technology, Hangzhou 310014, China

Supporting Information

ABSTRACT: Two-dimensional (2D) metal–organic framework (MOF) nanosheets are attracting increasing research interest. Here, for the first time, we report the facile synthesis of 2D porphyrin paddlewheel framework-3 (PPF-3) MOF nanosheets with thickness of ca. 12–43 nm. Through the simultaneous sulfidation and carbonization of PPF-3 MOF nanosheets, we have prepared the 2D nanocomposite of $CoS_{1.097}$ nanoparticles (NPs) and nitrogen-doped carbon, referred to as CoSNC, in which the $CoS_{1.097}$ NPs with size of ca. 10 nm are embedded in the nitrogen-doped carbon matrix. As a proof-of-concept application, the obtained 2D CoSNC nanocomposite is used as an electrode material for a supercapacitor, which exhibits a specific capacitance of 360.1 F g^{-1} at a current density of 1.5 A g^{-1}. Moreover, the composite electrode also shows high rate capability. Its specific capacitance delivered at a current density of 30.0 A g^{-1} retains 56.8% of the value at 1.5 A g^{-1}.

Two-dimensional (2D) materials have attracted tremendous research attention in recent years due to their unique physical and chemical properties.[1−4] Their high aspect ratio, originating from their large lateral dimension and nanometer thickness, makes them ideal for various applications in electronics, energy storage, and gas separation.[1−3] Typical 2D nanomaterials with promising properties, such as graphene[1−3] and transition metal dichalcogenides,[4] have been intensively investigated. As a newly developed material, the 2D metal–organic framework (MOF) nanosheet, a new member of the 2D material family, has attracted increasing research interest.[5−7] As known, MOFs are crystalline porous architectures constructed by coordination of metal ions or clusters with polytopic organic ligands.[8−11] Compared to three-dimensional (3D) bulk MOF crystals with highly ordered pores, the 2D MOF nanosheets exhibit some advantages, such as larger surface area and more accessible active sites on their surfaces due to their specific 2D morphology.[5−7] Conventionally, MOF nanosheets are prepared by the exfoliation of bulk MOF materials[5,12,13] or by direct bottom-up synthesis, including three-layer synthesis strategy,[6] layer-by-layer growth,[14,15] and our recently developed surfactant-assisted synthesis which allows for the high-yield synthesis of MOF nanosheets with thickness of less than 10 nm.[7]

As known, MOFs can be easily converted to metal oxides, highly porous carbon, and metal oxides/carbon, metal phosphides/carbon, or metal sulfides/carbon hybrid materials after the thermal treatment.[16−20] In this Communication, for the first time, we demonstrate the preparation of 2D porphyrin paddlewheel framework-3 (PPF-3) MOF nanosheets by using our recently developed surfactant-assisted synthetic method.[7] Through the simultaneous sulfidation and carbonization of PPF-3 MOF nanosheets, the 2D nanocomposite of $CoS_{1.097}$ nanoparticles (NPs) and nitrogen-doped carbon, referred to as CoSNC, is obtained. As a proof-of-concept application, the prepared 2D CoSNC nanocomposite is used as an electrode material for supercapacitors.

The synthesis of 2D PPF-3 nanosheets with controlled thickness is schematically shown in Figure 1a. During the

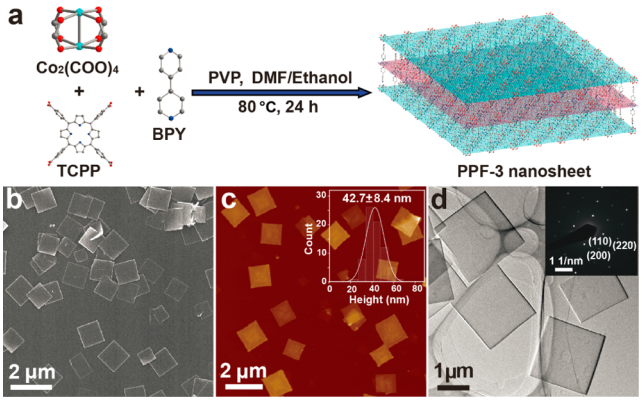

Figure 1. (a) Schematic illustration of the synthesis process of PPF-3 nanosheets. (b) SEM image of PPF-3 nanosheets. (c) AFM image of PPF-3 nanosheets. Inset: Statistical analysis of the thickness of 75 PPF-3 nanosheets measured in AFM images. (d) TEM image of PPF-3 nanosheets. Inset: SAED pattern of PPF-3 nanosheets.

Received: March 9, 2016
Published: May 20, 2016

DOI: 10.1021/jacs.6b02540
J. Am. Chem. Soc. 2016, 138, 6924–6927

experiment, the surfactant molecule, polyvinylpyrrolidone (PVP), was selectively attached onto the surface of PPF-3 MOFs, which controlled the vertical growth of PPF-3 MOF crystals, resulting in the formation of 2D PPF-3 nanosheets (see experimental details in the Supporting Information (SI)). In the obtained PPF-3 nanosheet, one 5,10,15,20-tetrakis(4-carboxylphenyl)porphyrin (TCPP) ligand is metalated by one cobalt ion and linked by four $Co_2(COO)_4$ paddlewheel metal nodes to form a "checkerboard-like" layered structure, which is further pillared by 4,4′-bipyridine (BPY) molecules in an AB stacking pattern to form the final structure with space group of *I*4/*mmm* (Figure S1).[21]

Scanning electron microscopy (SEM), transmission electron microscopy (TEM), atomic force microscopy (AFM), and powder X-ray diffraction (XRD) were used to characterize the synthesized PPF-3 nanosheets. The square-like sheet structure of obtained PPF-3 MOF with lateral size of 1.5 ± 0.3 μm (Figure 1b and Figure S2) and thickness of 42.7 ± 8.4 nm (Figure 1c) was obtained. The selected-area electron diffraction (SAED) pattern collected along the [001] axis gives diffraction spots (inset in Figure 1d) which are attributed to the (110), (220), and (200) planes of PPF-3 nanosheets, confirming the crystal structure. In addition, the typical peaks of PPF-3 nanosheets in the XRD spectrum (Figure S3a) match well with those of bulk PPF-3 MOFs (Figure S3a,b), indicating the tetragonal structure of PPF-3 nanosheets with good crystallinity. Importantly, the thickness of PPF-3 nanosheets can be tuned (see experimental details in SI); when the concentration of starting materials was decreased, 2D square-like ultrathin PPF-3 nanosheets were obtained (Figure S4). The SAED pattern collected along the [001] axis gives diffraction spots (inset in Figure S4b) confirming the crystal structure of these ultrathin PPF-3 nanosheets. The AFM measurement confirms that the thickness of ultrathin PPF-3 nanosheets is 11.9 ± 4.2 nm (Figure S4c,d).

Importantly, the synthesized 2D PPF-3 nanosheets can be converted to 2D CoSNC nanocomposites through the simultaneous sulfidation and carbonization process (Figure 2a; see experimental details in SI). The composition of the 2D CoSNC nanocomposite is confirmed by the XRD pattern (Figure 2b), in which all peaks can be indexed to a broad diffraction peak (002) of carbon and the $CoS_{1.097}$, consistent with those of the *β*-$CoS_{1.097}$ phase (JCPDS No. 19-366) with hexagonal structure.[22]

Note that the thickness of PPF-3 MOFs, used as precursors, is critically important for the synthesis of CoSNC composites for further supercapacitor application. In a control experiment, if bulk PPF-3 MOFs were used as the precursor, the obtained bulk CoSNC composites (Figure S5) would hinder the electron/ion transport, leading to the poor electrochemical performance. On the other hand, after the thermal treatment of ultrathin PPF-3 nanosheets with thickness of 11.9 ± 4.2 nm, the 2D nanostructures were destroyed (Figure S6). Fortunately, when PPF-3 nanosheets with thickness of 42.7 ± 8.4 nm were used as precursors, the obtained CoSNC nanocomposites can still keep the 2D square-like morphology with lateral size of 1.4 ± 0.3 μm (Figure S7) and thickness of 24.5 ± 6.4 nm (Figure 2c). Compared to the original PPF-3 nanosheets (Figure 1c), the thickness of 2D CoSNC nanocomposites (Figure 2c) decreased, which might arise from the carbonization of PPF-3 nanosheets. Furthermore, the 2D CoSNC nanocomposite was characterized by TEM (Figure 2d,e) and high-angle dark-field scanning TEM (HAADF-STEM) (Figure 2f). An enlarged

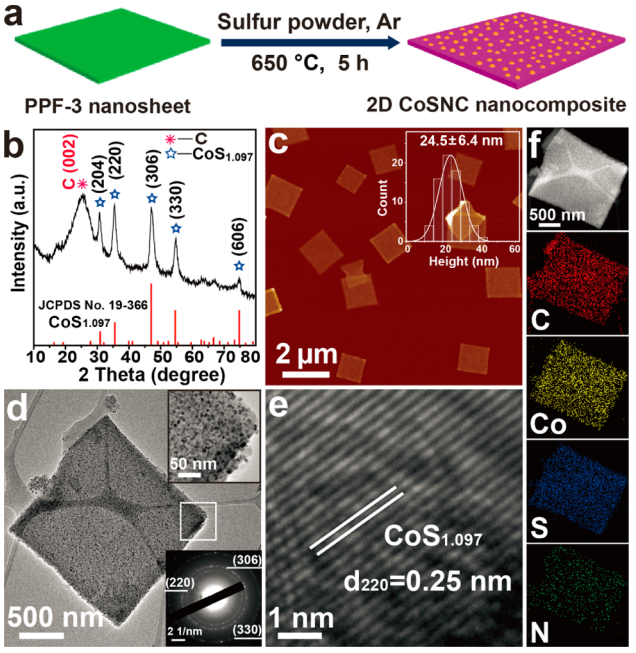

Figure 2. (a) Schematic illustration for the synthesis process of 2D CoSNC nanocomposites. (b) XRD pattern of 2D CoSNC nanocomposites. (c) AFM image of 2D CoSNC nanocomposites. Inset: Statistical analysis of the thickness of 75 2D CoSNC nanocomposites measured in AFM images. (d) TEM image of a typical 2D CoSNC nanocomposite. Top inset: TEM image taken from the white square in the main panel. Bottom inset: SAED pattern of 2D CoSNC nanocomposites. (e) HRTEM image of 2D CoSNC nanocomposites. (f) Annual dark-field TEM image of 2D CoSNC nanocomposites and the corresponding EDX elemental mapping images of elements C, Co, S, and N.

TEM image taken from the edge of 2D CoSNC nanocomposite (top inset in Figure 2d) confirms the existence of NPs with size of 9.9 ± 2.7 nm embedded in the 2D carbon matrix (Figure S8a,b). The SAED pattern (bottom inset in Figure 2d) matches well with that of typical $CoS_{1.097}$.[22] In addition, the HRTEM image (Figure 2e) gives very clear crystalline planes with a *d*-spacing of 0.25 nm, which can be ascribed to the (220) plane of $CoS_{1.097}$, further confirming that highly crystalline $CoS_{1.097}$ NPs were obtained.[22] A typical HAADF-STEM image of 2D CoSNC nanocomposite shows uniform dispersion of the C, Co, S, and N elements in the whole nanocomposite (Figure 2f), suggesting the distribution of $CoS_{1.097}$ NPs in the nitrogen-doped carbon matrix. The presence of these elements can be further confirmed by the energy-dispersive X-ray (EDX) spectra (Figure S8c). Therefore, during the thermal process, the cobalt ions in the PPF-3 nanosheets have been converted to $CoS_{1.097}$ NPs, while the nitrogen-rich organic ligands (TCPP and BPY), which contain both carbon and nitrogen, were *in situ* carbonized to form the nitrogen-doped carbon matrix. Since cobalt ions are uniformly distributed in the PPF-3 nanosheets and ligands are linked by cobalt paddlewheel metal nodes, a uniform dispersion of $CoS_{1.097}$ NPs in the nitrogen-doped carbon matrix with strong adsorption is achieved after the simultaneous carbonization of the frameworks and sulfidation of cobalt ions in the PPF-3 nanosheets with thermal annealing.

Moreover, X-ray photoelectron spectroscopy (XPS) was used to characterize the obtained 2D CoSNC nanocomposites (Figure 3). The C 1s core level peak can be resolved into three components centered at 284.4, 285.0, and 288.4 eV,

DOI: 10.1021/jacs.6b02540
J. Am. Chem. Soc. 2016, 138, 6924−6927

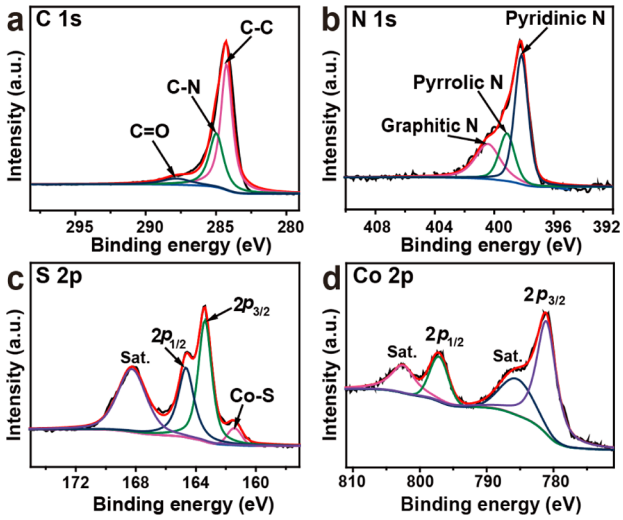

Figure 3. High-resolution (a) C 1s, (b) N 1s, (c) S 2p, and (d) Co 2p XPS spectra of 2D CoSNC nanocomposites.

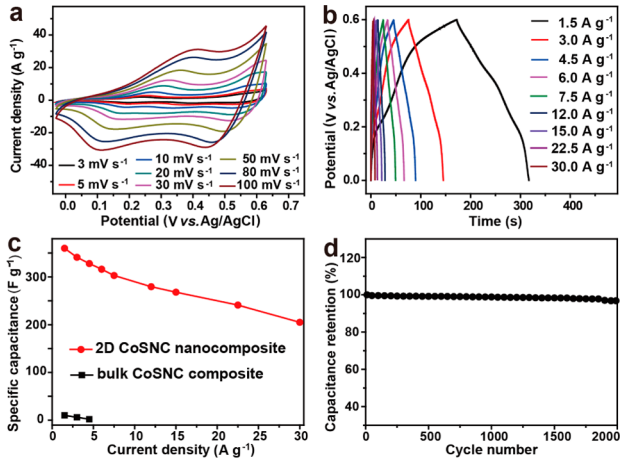

Figure 4. (a) CV and (b) galvanostatic charge/discharge curves of the 2D CoSNC nanocomposite electrode measured in 2.0 M KOH. (c) Specific capacitance of 2D CoSNC nanocomposite and bulk CoSNC composite as a function of current density. (d) Cycling stability of 2D CoSNC nanocomposite electrode measured at 12.0 A g^{-1} in 2.0 M KOH.

corresponding to the C−C, C−N, and C═O bonds, respectively (Figure 3a).[23−27] The existence of C−N bond further confirmed the nitrogen-doping in the carbon matrix.[23] The N 1s XPS spectrum can be deconvoluted into three peaks centered at 398.2, 399.0, and 400.4 eV (Figure 3b), which are consistent with the pyridinic, pyrrolic and graphitic nitrogen atoms doped in the carbon matrix.[23−27] Obviously, doping nitrogen into the carbon matrix originates from the nitrogen atoms existing in the ligands of PPF-3 nanosheets.[23,25] As shown in Figure 3c, the deconvolution of the S 2p peak illustrated the presence of S $2p_{3/2}$ and S $2p_{1/2}$ spin−orbit doublet.[28] Another peak centered at 161.4 eV could be assigned to Co-deficient nonstoichiometric sulfides.[29] In Figure 3d, the Co 2p spectrum showed two characteristic peaks, corresponding to $2p_{3/2}$ and $2p_{1/2}$.[28] Moreover, the Raman spectrum of 2D CoSNC nanocomposites shows the intensive G band (Figure S8d), indicating the presence of graphitic carbon.[25]

Due to the unique 2D morphology and the $CoS_{1.097}$ NPs dispersing in the nitrogen-doped carbon matrix, the 2D CoSNC nanocomposites (Figure 2) might have good supercapacitive performance. As shown in Figure 4a, all the cyclic voltammetry (CV) curves of 2D CoSNC nanocomposite electrode exhibited rectangular-like shapes with distinct redox peaks, which indicates the capacitance characteristics are governed by both Faradaic redox reactions and electric double-layer capacitor (EDLC).[22,29] Meanwhile, its galvanostatic charge/discharge curves exhibited approximately symmetric shapes with small plateaus (Figure 4b). It is worth noting that even though the 2D CoSNC nanocomposite contains only 21.0 wt% of $CoS_{1.097}$ based on thermogravimetric analysis (TGA) (Figure S9), it delivered much higher specific capacitance (C_s) than the bulk composite electrode (Figure 4c). For example, the 2D CoSNC nanocomposite electrode gave a C_s value as high as 360.1 F g^{-1} at the current density of 1.5 A g^{-1}, which is almost 34 times that of the bulk CoSNC composite electrode (10.6 F g^{-1}). This result clearly demonstrates the structural advantage of the 2D CoSNC nanocomposite, which provided more active sites as compared to its bulk counterpart. Importantly, the 2D CoSNC nanocomposite also exhibited good rate capability (Figure 4c). The C_s values at relatively high current densities of 6.0, 12.0, and 15.0 A g^{-1} were 87.9%, 77.7%, and 74.3% of that at 1.5 A g^{-1}, respectively. Even at a very high current density of 30.0 A g^{-1}, the C_s still maintains a value 56.8% of that at 1.5 A g^{-1}. Moreover, a C_s retention of ∼90% was achieved for the 2D CoSNC nanocomposite electrode after 2000 charge/discharge cycles at a current density of 12.0 A g^{-1}, indicating good cycling performance (Figure 4d). Compared to the previous reported electrode materials, including MOF-derived nanomaterials and cobalt sulfide-based materials, our 2D CoSNC nanocomposite electrode possessed comparable or even better performance (Table S1), especially showing an excellent high-rate performance.

The aforementioned excellent performance of the 2D CoSNC nanocomposite electrode may arise from two reasons. First, the ultrathin 2D CoSNC nanocomposite with thickness of 24.5 ± 6.4 nm (Figure 2c) effectively shortened the diffusion path of electrolyte ions, provided a fast ion/electron transport way, and increased the density of active sites for the redox reaction. Second, the nitrogen-doped carbon matrix served as a conductive path for the rapid electron transport between the 2D CoSNC nanocomposite and current collector, which enhanced the electrochemical kinetics. Therefore, our 2D CoSNC nanocomposite with unique 2D hybrid structure and highly synergistic energy-storage properties led to excellent supercapacitive performance.

In summary, by using our recently developed surfactant-assisted synthetic approach, 2D PPF-3 nanosheets have been synthesized. The 2D CoSNC nanocomposites were obtained through the simultaneous sulfidation and carbonization of PPF-3 nanosheets. As a proof-of-concept application, the obtained 2D CoSNC nanocomposite was successfully used as an electrode for a supercapacitor, which showed high capacitance, high rate, and long cycling performance. Our work indicates that the MOF nanosheets can be used to prepare various 2D functional hybrid materials due to their unique structure and functionalizable nature.

■ ASSOCIATED CONTENT

Supporting Information

The Supporting Information is available free of charge on the ACS Publications website at DOI: 10.1021/jacs.6b02540.

DOI: 10.1021/jacs.6b02540
J. Am. Chem. Soc. 2016, 138, 6924−6927

Detailed methods and further characterizations, Figures S1−S9, and Table S1 (PDF)

AUTHOR INFORMATION

Corresponding Author

*hzhang@ntu.edu.sg

Author Contributions

‖F.C. and M.Z. contributed equally.

Notes

The authors declare no competing financial interest.

ACKNOWLEDGMENTS

This work was supported by the Fundamental Research Funds for the Central Universities, China (No. 2662015PY163), National Natural Science Foundation of China (No. 2130-3064), and Wuhan Chenguang Science and Technology Project for Young Experts, China (2015070404010192). It was also supported by MOE under AcRF Tier 2 (ARC 26/13, No. MOE2013-T2-1-034; ARC 19/15, No. MOE2014-T2-2-093; MOE2015-T2-2-057) and AcRF Tier 1 (RG5/13), and by NTU under Start-Up Grant M4081296.070.500000 in Singapore.

REFERENCES

(1) Dreyer, D. R.; Park, S.; Bielawski, C. W.; Ruoff, R. S. *Chem. Soc. Rev.* **2010**, *39*, 228.
(2) Novoselov, K. S.; Falko, V. I.; Colombo, L.; Gellert, P. R.; Schwab, M. G.; Kim, K. *Nature* **2012**, *490*, 192.
(3) Zhang, J.; Jiang, J.; Li, H.; Zhao, X. S. *Energy Environ. Sci.* **2011**, *4*, 4009.
(4) Acerce, M.; Voiry, D.; Chhowalla, M. *Nat. Nanotechnol.* **2015**, *10*, 313.
(5) Peng, Y.; Li, Y.; Ban, Y.; Jin, H.; Jiao, W.; Liu, X.; Yang, W. *Science* **2014**, *346*, 1356.
(6) Rodenas, T.; Luz, I.; Prieto, G.; Seoane, B.; Miro, H.; Corma, A.; Kapteijn, F.; Llabrés i Xamena, F. X.; Gascon, J. *Nat. Mater.* **2015**, *14*, 48.
(7) Zhao, M.; Wang, Y.; Ma, Q.; Huang, Y.; Zhang, X.; Ping, J.; Zhang, Z.; Lu, Q.; Yu, Y.; Xu, H.; Zhao, Y.; Zhang, H. *Adv. Mater.* **2015**, *27*, 7372.
(8) Deria, P.; Mondloch, J. E.; Karagiaridi, O.; Bury, W.; Hupp, J. T.; Farha, O. K. *Chem. Soc. Rev.* **2014**, *43*, 5896.
(9) Furukawa, H.; Cordova, K. E.; O'Keeffe, M.; Yaghi, O. M. *Science* **2013**, *341*, 1230444.
(10) Zhou, H. C.; Long, J. R.; Yaghi, O. M. *Chem. Rev.* **2012**, *112*, 673.
(11) Zhou, H.-C.; Kitagawa, S. *Chem. Soc. Rev.* **2014**, *43*, 5415.
(12) Li, P. Z.; Maeda, Y.; Xu, Q. *Chem. Commun.* **2011**, *47*, 8436.
(13) Gallego, A.; Hermosa, C.; Castillo, O.; Berlanga, I.; Gómez, C. J.; Mateo, E.; Martínez, J. I.; Flores, F.; GómezNavarro, C.; GómezHerrero.; et al. *Adv. Mater.* **2013**, *25*, 2141.
(14) Makiura, R.; Motoyama, S.; Umemura, Y.; Yamanaka, H.; Sakata, O.; Kitagawa, H. *Nat. Mater.* **2010**, *9*, 565.
(15) Motoyama, S.; Makiura, R.; Sakata, O.; Kitagawa, H. *J. Am. Chem. Soc.* **2011**, *133*, 5640.
(16) Wang, Z.; Liu, Y.; Gao, C.; Jiang, H.; Zhang, J. *J. Mater. Chem. A* **2015**, *3*, 20658.
(17) Cao, X.; Zheng, B.; Shi, W.; Yang, J.; Fan, Z.; Luo, Z.; Rui, X.; Chen, B.; Yan, Q.; Zhang, H. *Adv. Mater.* **2015**, *27*, 4695.
(18) Wu, R.; Wang, D. P.; Rui, X.; Liu, B.; Zhou, K.; Law, A. W. K.; Yan, Q.; Wei, J.; Chen, Z. *Adv. Mater.* **2015**, *27*, 3038.
(19) You, B.; Jiang, N.; Sheng, M. L.; Gul, S.; Yano, J.; Sun, Y. *Chem. Mater.* **2015**, *27*, 7636.
(20) Salunkhe, R.; Tang, J.; Kamachi, Y.; Nakato, T.; Kim, J.; Yamauchi, Y. *ACS Nano* **2015**, *9*, 6288.
(21) Choi, E. Y.; Barron, P. M.; Novotny, R. W.; Son, H. T.; Hu, C.; Choe, W. *Inorg. Chem.* **2009**, *48*, 426.
(22) Qu, B.; Chen, Y.; Zhang, M.; Hu, L.; Lei, D.; Lu, B.; Li, Q.; Wang, Y.; Chen, L.; Wang, T. *Nanoscale* **2012**, *4*, 7810.
(23) Maldonado, S.; Morin, S.; Stevenson, K. J. *Carbon* **2006**, *44*, 1429.
(24) Li, X.; Wang, H.; Robinson, J.; Sanchez, H.; Diankov, G.; Dai, H. *J. Am. Chem. Soc.* **2009**, *131*, 15939.
(25) Li, B.; Dai, F.; Xiao, Q. F.; Yang, L.; Zhang, C. M.; Cai, M. *Energy Environ. Sci.* **2016**, *9*, 102.
(26) Liu, M.; Zhang, L.; Han, P.; Han, X.; Du, H.; Yue, X.; Zhang, Z.; Zhang, H.; Cui, G. *Part. Part. Syst. Charact.* **2015**, *32*, 1006.
(27) Zhang, B.; Cui, G.; Zhang, K.; Zhang, L.; Han, P.; Dong, S. *Electrochim. Acta* **2014**, *150*, 15.
(28) Liu, S.; Wang, J.; Wang, J.; Zhang, F.; Liang, F.; Wang, L. *CrystEngComm* **2014**, *16*, 814.
(29) Wu, R.; Wang, D.; Kumar, V.; Zhou, K.; Law, A. W. K.; Lee, P.; Lou, J.; Chen, Z. *Chem. Commun.* **2015**, *51*, 3109.

DOI: 10.1021/jacs.6b02540
J. Am. Chem. Soc. 2016, 138, 6924−6927